Chinese Chemical Letters 32 (2021) 2904–2908

Contents lists available at ScienceDirect

Chinese Chemical Letters

journal homepage: www.elsevier.com/locate/cclet

Communication

# Enhancing the performances of all-small-molecule ternary organic solar cells *via* achieving optimized morphology and 3D charge pathways

Yanhong Chang[a,c,1], Jing Li[a,b,c,1], Yilin Chang[b,d], Yixiao Zhang[b,d], Jianqi Zhang[b], Kun Lu[b,d,*], Xiangnan Sun[b,d,e,f,*], Zhixiang Wei[b,d,*]

[a] Department of Environmental Science and Engineering, University of Science and Technology Beijing, Beijing 100083, China
[b] CAS Key Laboratory of Nanosystem and Hierarchical Fabrication, CAS Center for Excellence in Nanoscience, National Center for Nanoscience and Technology, Beijing 100190, China
[c] Beijing Key Laboratory of Resource-oriented Treatment of Industrial Pollutants, Beijing 100083, China
[d] University of Chinese Academy of Sciences, Beijing 100049, China
[e] Shandong First Medical University & Shandong Academy of Medical Sciences, Taian 271016, China
[f] School of Materials Science and Engineering, Zhengzhou University, Zhengzhou 450001, China

ARTICLE INFO

*Article history:*
Received 30 November 2020
Received in revised form 15 March 2021
Accepted 24 March 2021
Available online 26 March 2021

*Keywords:*
All-small-molecule
Ternary organic solar cells
Alloyed acceptor
Morphology optimization
3D charge pathways

ABSTRACT

With the emergence of non-fullerene acceptors (NFAs), the power conversion efficiencies (PCEs) of all-small-molecule organic solar cells (ASM-OSCs) have been significantly improved. However, due to the strong crystallinities of small molecules, it is much more challenging to obtain the ideal phase separation morphology and efficient charge transport pathways for ASM-OSCs. Here, a high-efficiency ternary ASM-OSC has been successfully constructed based on H11/IDIC-4F system by introduction of IDIC with a similar backbone as IDIC-4F but weak crystallinity. Notably, the addition of IDIC has effectively suppressed large-scale phase aggregation and optimized the morphology of the blend film. More importantly, the molecular orientation has also been significantly adjusted, and a mixed face-on and edge-on orientation has formed, thus establishing a more favorable three-dimensional (3D) charge pathways in the active layer. With these improvements, the enhanced short-circuit current density ($J_{SC}$) and fill factor (FF) of the ternary system have been achieved. In addition, because of the high lowest unoccupied molecular orbital (LUMO) energy level of IDIC as well as the alloyed structure of the IDIC and IDIC-4F, the promoted open circuit voltage ($V_{OC}$) of the ternary system has also been realized.


In recent years, a great deal of progress has been made in organic solar cells (OSCs) owing to the development of new photovoltaic materials and the optimization of device fabrication [1–10]. Up to now, power conversion efficiencies (PCEs) of over 18% have been achieved for single-junction OSCs [11]. It is worth mentioning that most of the high-efficient OSCs are based on the copolymers as donors [12,13]. However, donor polymers have disadvantage of synthetic complexity, batch-to-batch variation and purification difficulty, severely restricting further industrial applications of OSCs [14,15]. In contrast, small molecules possess distinctive superiorities relative to polymers in definite chemical structures, high purity and negligible batch-difference, which are highly suited to larger-scale processes [16–20]. Although the PCEs of all-small-molecule organic solar cells (ASM-OSCs) have reached more than 15% [21–23] by virtue of the introduction of non-fullerene acceptors (NFAs) and the application of ternary strategy [22,23], there are still obvious gaps compared with polymer solar cells, no matter in photovoltaic performance or the scale of research. The main reasons for the relatively low efficiencies of ASM-OSCs can be attributed to the strong aggregation behavior of small molecules, which is not conducive to the formation of ideal morphologies and efficient charge transport pathways. To address these challenges is becoming an increasingly urgent for the field.

A series of studies have demonstrated that introducing the third-component acceptor into ASM-OSCs is an effective strategy to optimize the morphology and improve charge transport for the

* Corresponding authors at: CAS Key Laboratory of Nanosystem and Hierarchical Fabrication, CAS Center for Excellence in Nanoscience, National Center for Nanoscience and Technology, Beijing 100190, China.
*E-mail addresses:* lvk@nanoctr.cn (K. Lu), sunxn@nanoctr.cn (X. Sun), weizx@nanoctr.cn (Z. Wei).
[1] These authors contributed equally to this work.

https://doi.org/10.1016/j.cclet.2021.03.067

newly-constructed ternary system [22,24–29]. For example, Zhou *et al*. reported a high-efficiency ASM ternary system, which is composed of small molecule donor (BTR), a NFA (NITI) and a fullerene acceptor ($PC_{71}BM$) as the third component. With the combination of fullerene and non-fullerene acceptors, a hierarchical morphology consisting of a $PC_{71}BM$ transporting highway and an intricate non-fullerene phase-separated pathway has been successfully achieved, which significantly facilitates the charge carrier generation and transport [30]. Compared with fullerene acceptors, NFAs are more attractive in the tunable absorption spectra, energy levels and crystallinity [31–37]. However, the report about ternary ASM-OSCs with two non-fullerene acceptors is extremely rare. Until recently, Nian *et al*. used a highly crystalline NFA (4TIC) as the additional acceptor to construct the ternary ASM-OSCs. 4TIC has played important role not only in enhancing the crystallinity of the ternary blend, but also in maintaining the favorable face-on orientation in the proper multi-length scale morphology, all of which dominate the improvements of overall performance for the ternary system [23]. These results indicate that the additional acceptor, especially NFA, has great potential in constructing high-performance ternary ASM-OSCs which is worth further exploration.

In this study, we have constructed a high-efficiency ternary ASM-OSC based on the binary system of H11/IDIC-4F [38] by introducing IDIC as the third component, with a similar backbone structure as IDIC-4F, but high lowest unoccupied molecular orbital (LUMO) energy level and weak crystallinity [39–42]. The obvious difference between our work and Nian's report is that both the morphology and molecular orientation have changed dramatically after the addition of IDIC. On one hand, the root-mean-square (RMS) roughness of the ternary blend film has been significantly decreased, leading to a much smoother surface morphology. On the other hand, there has been a mixed face-on and edge-on orientation in the ternary blend film, thus creating a type of three-dimensional (3D) charge pathways for the improved short-circuit current density ($J_{SC}$) and fill factor (FF). Moreover, since IDIC and IDIC-4F can form an alloyed structure in the ternary blend, so the addition of IDIC makes it great for obtaining the enhanced open circuit voltage ($V_{OC}$) for the ternary ASM-OSC. Consequently, the PCE of the H11/IDIC-4F based device has enhanced from 10.2% to 11.9% after the addition of IDIC. This work demonstrates that the morphology and molecular orientation of ASM-OSCs can be finely controlled by the introduction of additional NFA with relatively weak crystallinity, which provides an effective avenue to promote the device performance for ASM-OSCs.

The chemical structures of H11, IDIC and IDIC-4F are presented in Fig. 1a. The normalized absorption spectra of the H11, IDIC and IDIC-4F solution and neat film are displayed in Fig. S1 (Supporting information) and Fig. 1b, respectively. H11 shows main absorption from 400 nm to 700 nm with the maximum absorption peaks at 558 nm and 600 nm. IDIC and IDIC-4F have similar absorption characteristics. But compared with IDIC, IDIC-4F exhibits red-shifted absorption edge due to the incorporation of fluorine atoms. The shoulder peaks are observed in neat films of both IDIC and IDIC-4F, suggesting IDIC and IDIC-4F possess strong $\pi$-$\pi$ interactions in the solid state [40]. Moreover, excellent absorption complementarity exists between H11 and IDIC/IDIC-4F. As shown in Fig. 1c, the LUMO/highest occupied molecular orbital (HOMO) energy levels of H11, IDIC and IDIC-4F are −3.03 eV/−5.31 eV [39], −3.94 eV/−5.71 eV and −4.05 eV/−5.77 eV, respectively. The energy levels of IDIC and IDIC-4F was measured by cyclic voltammetry and the results are shown in Fig. S2 (Supporting information). On one hand, the LUMO level offset between H11 and IDIC/IDIC-4F is about 0.9 eV, which is large enough for exciton dissociation and charge transfer [43,44]. On the other hand, because $V_{OC}$ is proportional to the energy level offset between the HOMO level of donor and the LUMO level of acceptor [45,46], IDIC-based device can display higher $V_{OC}$ than that of IDIC-4F-based device according to its slightly higher LUMO energy level.

The devices with the conventional structure of ITO/PEDOT:PSS/active layer/PDINO/Ag were constructed. The details of the device fabrication were described in supporting information. The H11/IDIC-based binary device exhibited a slightly higher PCE of 9.9% ($V_{OC}$ = 0.99 V, $J_{SC}$ =15.68 mA/cm$^2$, FF = 64.1%) compared with Bin's result of 9.73% [39]. With the same D/A ratio, the H11/IDIC-4F-based binary device delivered a PCE of 10.2% ($V_{OC}$ = 0.81 V, $J_{SC}$ =17.76 mA/cm$^2$, FF = 70.7%) with the Donor/Acceptor (D/A) ratio of 1.7:1, which is roughly equivalent to the PCE of 10.4% reported by Janssen's group [38]. Such a tiny gap might be attributed to the different D/A ratio with their report. Notably, for the H11/IDIC-4F-based system, although the $V_{OC}$ is far below that of H11/IDIC-based device, both the $J_{SC}$ and FF are significantly improved. Considering their respective advantages of the two binary systems, IDIC was added into H11/IDIC-4F-based system as the third component for constructing high-performance ternary OSCs. By adjusting the content of IDIC, an optimal PCE of 11.9% with a moderate $V_{OC}$ of 0.89 V and significantly enhanced $J_{SC}$ of 18.48 mA/cm$^2$ and FF of 72.3% for the ternary OSC was finally obtained. The corresponding photovoltaic parameters are summarized in Table 1, and the

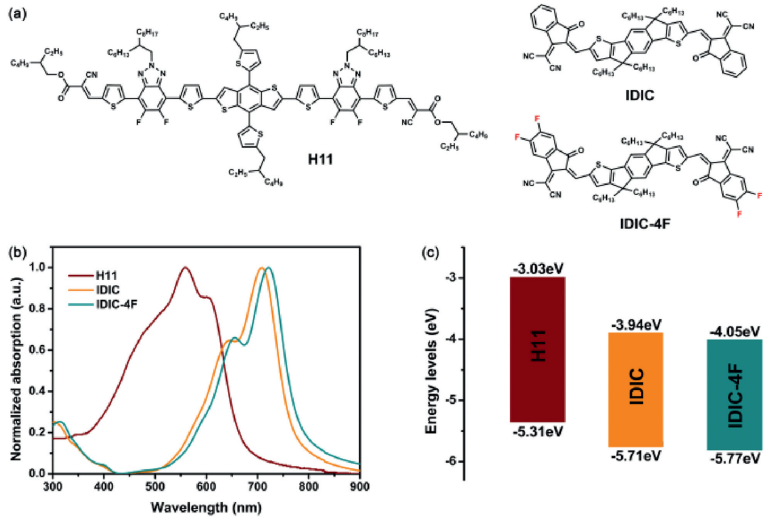


**Fig. 1.** (a) The chemical structure of H11, IDIC and IDIC-4F. (b) Normalized absorption of H11, IDIC and IDIC-4F in neat films. (c) Energy level diagram of H11, IDIC and IDIC-4F.

**Table 1**
Photovoltaic parameters of the binary and the optimized ternary ASM-OSCs.[a]

| H11:IDIC:IDIC-4F | $V_{OC}$ (V) | $J_{SC}$ (mA/cm$^2$) | FF (%) | PCE (%) |
|---|---|---|---|---|
| 1.7:1:0 | 0.99 (0.98 ± 0.01) | 15.68 (15.69 ± 0.37) | 64.1 (63.6 ± 1.30) | 9.9 (9.8 ± 0.08) |
| 1.7:0.4:0.6 | 0.89 (0.90 ± 0.01) | 18.48 (18.18 ± 0.25) | 72.3 (72.0 ± 0.66) | 11.9 (11.7 ± 0.14) |
| 1.7:0:1 | 0.81 (0.81 ± 0.01) | 17.76 (17.89 ± 0.43) | 70.7 (69.8 ± 1.17) | 10.2 (10.1 ± 0.09) |

[a] The average and standard deviation values of ten devices was listed in the parenthesis.

detailed photovoltaic performances of the binary and ternary devices with different D/A ratios are shown in Tables S1–S3 (Supporting information). Fig. 2a shows related current density *versus* voltage (*J–V*) curves under AM 1.5 G, 100 mW/cm$^2$. As shown in Fig. S3 (Supporting information), the $V_{OC}$s of the ternary OSCs present a linear-increase trend with the increase of the content of IDIC, demonstrating that the two acceptors can form an alloyed structure due to their almost the same molecular backbone [47,48]. To confirm IDIC and IDIC-4F can form an alloyed structure, differential scanning calorimetry (DSC) measurements was employed. As shown in Fig. S4 (Supporting information), the highest melting point of IDIC and IDIC-4F are located at 296.0 °C and 293.1 °C, respectively. It is clearly that the melting peaks of the blend happened moved in the low temperature direction. The results demonstrate that IDIC and IDIC-4F form the alloyed receptor [43]. Moreover, the reasons accounting for the improved $J_{SC}$ and FF of the ternary system will be further analyzed in the following parts. The external quantum efficiency (EQE) curves of the binary and the optimized ternary ASM-OSCs are shown in Fig. 2b. Compared with the two binary devices, the EQE values of the optimized ternary device are obviously enhanced in a wide range of 435–720 nm, indicating more of the light can be converted into the current after introduction of IDIC into the binary systems. The calculated $J_{SC}$ values according to the EQE spectra for H11/IDIC, H11/IDIC-4F and H11/IDIC/IDIC-4F based devices are 15.329, 17.277 and 17.934 mA/cm$^2$, respectively. The errors between the calculated $J_{SC}$ values and the measured $J_{SC}$ values are less than 5%, meaning that the photovoltaic performances of the binary and ternary OSCs are reliable.

For studying the effects of introduction of IDIC on the charge recombination, *J-V* curves were measured under different light intensities ($P_{light}$). Normally, a slope value can be obtained by fitting the $V_{OC}$ and ln$P_{light}$ according to the relation $V_{OC} \propto kT/q \ln P_{light}$ ($k$ is the Boltzmann constant, $T$ is absolute temperature, and $q$ is elementary charge). If the slope value is much closer to 2 $kT/q$, trap-assisted recombination will be the dominant recombination mode. While if the slope value is much closer to 1 $kT/q$, bimolecular recombination will be more dominant [49]. From Fig. 2c, the slope values for the H11/IDIC-based system, H11/IDIC-4F-based system and the optimized ternary system can be calculated as 1.19 $kT/q$, 1.26 $kT/q$ and 1.29 $kT/q$, indicating these three systems are more influenced by bimolecular recombination. Then, the bimolecular recombination of three systems are investigated by fitting the $J_{SC}$ and ln $P_{light}$ according to the relation $J_{SC} \propto P_{light}^{\alpha}$, where $\alpha$ reflects status of the bimolecular recombination. Bimolecular recombination can be considered as negligible when $\alpha$ approach 1 [50]. As displayed in Fig. 2d, the fitted $\alpha$ values for the H11/IDIC-based system, H11/IDIC-4F-based system and the optimized ternary system are 1.102, 1.061 and 1.058, respectively. Obviously, the value of the optimized ternary system is closest to 1, suggesting that the bimolecular recombination in the ternary system is extremely weak. And the suppressed bimolecular recombination is in accordance with the improvements of $J_{SC}$ and FF for the optimized ternary system.

Charge carrier mobilities of the binary and the optimized ternary devices were assessed by a space-charge limited current (SCLC) method [51]. The corresponding device structure of hole-only or electron-only device is ITO/PEDOT:PSS/active layer/ Au or ITO/Al/ active layer/Al, respectively. The detailed measurements and charge carrier mobilities are shown in Fig. S5 and Table S4 (Supporting information). The hole and electron mobilities of the optimized ternary device are 7.40 × 10$^{-5}$ and 5.56 × 10$^{-5}$ cm$^2$ V$^{-1}$ s$^{-1}$, which

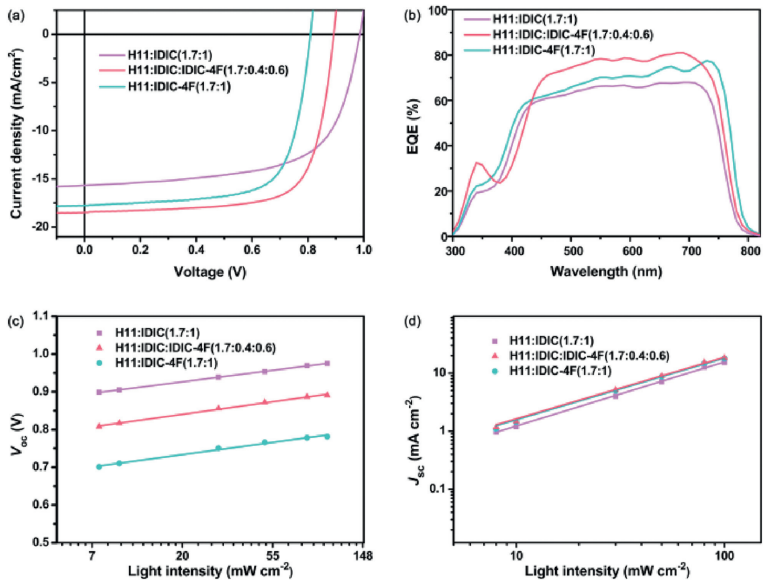


**Fig. 2.** (a) *J-V* curves. (b) EQE curves of the binary and the optimized ternary ASM-OSCs. (c) $V_{OC}$ dependence on light intensity of the binary and the optimized ternary ASM-OSCs. (d) $J_{SC}$ dependence on light intensity of the binary and the optimized ternary ASM-OSCs.

are slightly higher than those of the two binary devices, $1.98 \times 10^{-5}$ and $2.67 \times 10^{-5}$ $cm^2$ $V^{-1}$ $s^{-1}$ for H11/IDIC system and $4.03 \times 10^{-5}$ and $5.19 \times 10^{-5}$ $cm^2$ $V^{-1}$ $s^{-1}$ for H11/IDIC-4F system. The improved charge carrier mobilities partly explains the enhanced $J_{SC}$ and FF for the ternary system.

Atomic force microscopy (AFM) was employed for investigating the surface morphology of above three types of active layers. As shown in Fig. 3, the obvious aggregated domains exist in both H11/IDIC and H11/IDIC-4F-based active layers, resulting in the extremely high RMS roughness for H11/IDIC blend film (2.22 nm) and H11/IDIC-4F blend film (3.41 nm). While the RMS roughness of the optimized ternary blend film has been significantly decreased to 1.22 nm by the addition of IDIC to the binary film. As shown in Fig. S6 (Supporting information), the RMS roughness values for the ternary blend films with 30%, 50%, 60% and 70% IDIC were decreased to 1.39 nm, 1.33 nm, 1.74 nm and 1.68 nm, respectively. The results suggest that the blending of two phase is beneficial to reduce the RMS roughness for the blend films. Moreover, it can be clearly seen that the optimized ternary blend film exhibits much smoother surface characteristic, which is beneficial to obtain higher $J_{SC}$ and FF for the ternary system. The improvement of the morphology for the ternary system can be largely attributed to the good compatibility of the donor and two acceptors.

The crystallinity and molecular orientation of the binary and ternary blended films were analyzed by Grazing-incidence wide-angle X-ray scattering (GIWAXS). As shown in Fig. 4a, an obvious $\pi$-$\pi$ diffraction peak (010) appears in the in-plane (IP) direction, indicating the preferential edge-on orientation for H11/IDIC blend film. While from Fig. 4c, it can be concluded that H11/IDIC-4F blend film prefers to adopt the face-on orientation mainly because the $\pi$-$\pi$ diffraction peak (010) exists in the out-of-plane (OOP) direction. Interestingly, after adding the IDIC to the H11/IDIC-4F blend film, the $\pi$-$\pi$ diffraction peaks (010) appear in both IP and OOP direction (Fig. 4b and Fig. S7 in Supporting information), suggesting the mixed face-on and edge-on orientation in the ternary blend films. As reported in the previous study, the mixed orientation does help establish three-dimensional (3D) charge pathways, thus facilitating the vertical and parallel charge transports in BHJ films and leading to the enhanced $J_{SC}$, FF and PCE [52,53].

In summary, we have constructed a ternary ASM-OSCs though the addition of IDIC into H11/IDIC-4F-based binary system. By adjusting the contents of IDIC in the blend, the ternary ASM-OSCs presented an optimal PCE of 11.9%, which is superior to the performance of H11/IDIC-4F-based binary system (10.2%). Such a significant improvement is derived from the simultaneous

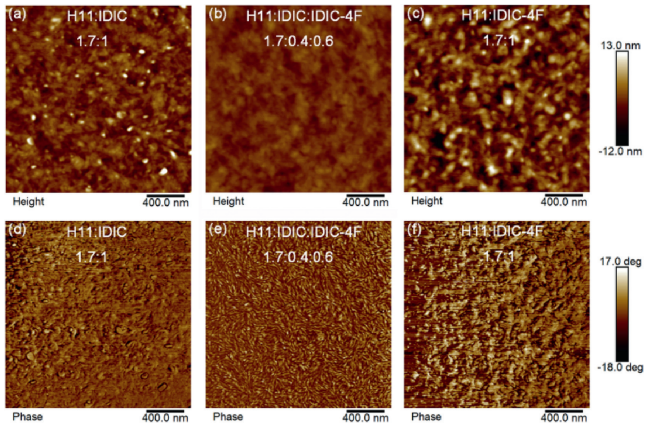


**Fig. 3.** (a-c) AFM height images and (d-f) AFM phase images of the binary and the optimized ternary ASM-OSCs.

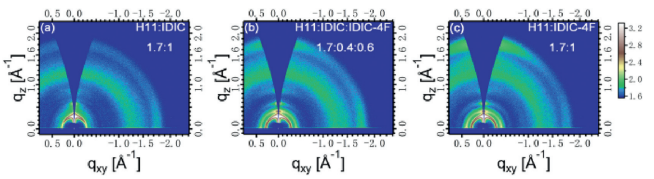


**Fig. 4.** (a-c) The 2D GIWAXS patterns of corresponding active layers for the binary and the optimized ternary ASM-OSCs.

growths of $V_{OC}$, $J_{SC}$ and FF for the ternary system. Benefiting from the relatively high LUMO level of IDIC and the good compatibility with IDIC-4F, the two acceptors blend can form an alloyed structure, enabling the enhanced $V_{OC}$ for the ternary device. Moreover, the optimized morphology and the mixed face-on and edge-on orientation were successfully obtained, mainly due to the weak crystallinity of IDIC and the orientation of IDIC-based binary system. All of these have contributed to the significant improvements of charge carrier mobilities, $J_{SC}$ and FF. These results demonstrate that introducing a homologous acceptor to a non-fullerene-based binary ASM-system may be an effective approach to achieve the excellent photovoltaic performances for the corresponding ternary ASM-OSCs.

## Declaration of competing interest

The authors report no declarations of interest.

## Acknowledgments

This work was supported financially by National Natural Science Foundation of China (Nos. 21822503, 51973043, 51822301 and 91963126), the Ministry of Science and Technology of the People's Republic of China (Nos. 2016YFA0200700, 2017YFA0206600), the Strategic Priority Research Program of the Chinese Academy of Sciences (No. XDB36020000), Beijing National Laboratory for Molecular Sciences (No. BNLMS201907), Youth Innovation Promotion Association, K. C. Wong Education Foundation, and the CAS Pioneer Hundred Talents Program. Yanhong Chang thanks National Environmental and Energy Base for International Science & Technology Cooperation.

## Appendix A. Supplementary data

Supplementary material related to this article can be found, in the online version, at doi:https://doi.org/10.1016/j.cclet.2021.03.067.

## References

[1] H. Wu, Q. Yue, Z. Zhou, et al., J. Mater. Chem. A 7 (2019) 15944–15950.
[2] T.W. Chen, C.C. Chang, Y.T. Hsiao, et al., ACS Appl. Mater. Interfaces 11 (2019) 31069–31077.
[3] X. Xu, L. Yu, H. Yan, et al., Energy Environ. Sci. 13 (2020) 4381–4388.
[4] J. Yuan, Y. Zhang, L. Zhou, et al., Adv. Mater. 31 (2019) 1807577.
[5] Y. Lin, J. Wang, Z.G. Zhang, et al., Adv. Mater. 27 (2015) 1170–1174.
[6] L. Arunagiri, Z. Peng, X. Zou, et al., Joule 4 (2020) 1790–1805.
[7] L. Zhan, S. Li, T.K. Lau, et al., Energy Environ. Sci. 13 (2020) 635–645.
[8] K. Jiang, Q. Wei, J.Y.L. Lai, et al., Joule 3 (2019) 3020–3033.
[9] J. Yuan, Y. Zhang, L. Zhou, et al., Joule 3 (2019) 1140–1151.
[10] N. Yan, C. Zhao, S. You, et al., Chin. Chem. Lett. 31 (2020) 643–653.
[11] Q. Liu, Y. Jiang, K. Jin, et al., Sci. Bull. 65 (2020) 272–275.
[12] Y. Cui, H. Yao, J. Zhang, et al., Adv. Mater. 32 (2020) 1908205.
[13] H. Sun, T. Liu, J. Yu, et al., Energy Environ. Sci. 12 (2019) 3328–3337.
[14] R. Zhou, Z. Jiang, C. Yang, et al., Nat. Commun. 10 (2019) 5393.
[15] Y. Sun, G.C. Welch, W.L. Leong, et al., Nat. Mater. 11 (2011) 44–48.
[16] R.-Z. Liang, Y. Zhang, V. Savikhin, et al., Adv. Energy Mater. 9 (2019) 1802836.
[17] H. Tang, H. Chen, C. Yan, et al., Adv. Energy Mater. 10 (2020) 2001076.
[18] D. Deng, Y. Zhang, J. Zhang, et al., Nat. Commun. 7 (2016) 13740.
[19] Q. Wu, D. Deng, K. Lu, et al., Chin. Chem. Lett. 28 (2017) 2065–2077.
[20] Y. Shi, C. Yang, H. Li, et al., Chin. Chem. Lett. 30 (2019) 906–910.

[21] J. Qin, C. An, J. Zhang, et al., Sci. China Mater. 63 (2020) 1142–1150.
[22] D. Hu, Q. Yang, H. Chen, et al., Energy Environ. Sci. 13 (2020) 2134–2141.
[23] L. Nian, Y. Kan, K. Gao, et al., Joule 4 (2020) 2223–2236.
[24] H. Zhang, X. Wang, L. Yang, et al., Adv. Mater. 29 (2017) 1703777.
[25] M. Zhang, J. Wang, F. Zhang, et al., Nano Energy 39 (2017) 571–581.
[26] Y. Huo, X.T. Gong, T.K. Lau, et al., Chem. Mater. 30 (2018) 8661–8668.
[27] S. Karuthedath, Y. Firdaus, R.Z. Liang, et al., Adv. Energy Mater. 9 (2019) 1901443.
[28] C. Xu, J. Wang, Q. An, et al., Nano Energy 66 (2019) 104119.
[29] F. Liu, C. Li, J. Li, et al., Chin. Chem. Lett. 31 (2020) 865–868.
[30] Z. Zhou, S. Xu, J. Song, et al., Nat. Energy 3 (2018) 952–959.
[31] F. Zhao, S. Dai, Y. Wu, et al., Adv. Mater. 29 (2017) 1700144.
[32] S. Dai, F. Zhao, Q. Zhang, et al., J. Am. Chem. Soc. 139 (2017) 1336–1343.
[33] Y. Guo, A. Zhang, C. Li, et al., Chin. Chem. Lett. 29 (2018) 371–373.
[34] Y. Zeng, R. Duan, Y. Guo, et al., Chin. Chem. Lett. 30 (2019) 211–216.
[35] S. Xie, J. Wang, R. Wang, et al., Chin. Chem. Lett. 30 (2019) 217–221.
[36] Y. Li, Y. Xu, F. Yang, et al., Chin. Chem. Lett. 30 (2019) 222–224.
[37] B. Liu, Y. Xu, D. Xia, et al., Acta Phys. Chim. Sin. 37 (2021) 2009056.
[38] H. Bin, I. Angunawela, B. Qiu, et al., Adv. Energy Mater. 10 (2020) 2001589.
[39] H. Bin, Y. Yang, Z.G. Zhang, et al., J. Am. Chem. Soc. 139 (2017) 5085–5094.
[40] Z. Li, R. Liang, J. Wang, et al., J. Phys. Chem. C 123 (2019) 28021–28026.
[41] H. Li, Q. Wu, R. Zhou, et al., Adv. Energy Mater. 9 (2018) 1803175.
[42] Q. Wu, D. Deng, J. Zhang, et al., Sci. China Chem. 62 (2019) 837–844.
[43] W. Su, Q. Fan, X. Guo, et al., Nano Energy 38 (2017) 510–517.
[44] C. Yang, Y. Sun, Q. Li, et al., J. Phys. Chem. Lett. 11 (2020) 927–934.
[45] G. Huang, J. Zhang, N. Uranbileg, et al., Adv. Energy Mater. 8 (2018) 1702489.
[46] Q. Ma, Z. Jia, L. Meng, et al., Nano Energy 78 (2020) 105272.
[47] Q. An, J. Zhang, W. Gao, et al., Small 14 (2018) 1802983.
[48] R. Lv, D. Chen, X. Liao, et al., Adv. Funct. Mater. 29 (2019) 1805872.
[49] S.R. Cowan, A. Roy, A.J. Heeger, Phys. Rev. B 82 (2010) 245207.
[50] A.K.K. Kyaw, D.H. Wang, V. Gupta, et al., ACS Nano 7 (2013) 4569–4577.
[51] A.B. Tamayo, B. Walker, T.Q. Nguyen, J. Phys. Chem. C 112 (2008) 11545.
[52] H. Bin, J. Yao, Y. Yang, et al., Adv. Mater. 30 (2018) 1706361.
[53] T. Kumari, S.M. Lee, S.H. Kang, et al., Energy Environ. Sci. 10 (2017) 258–265.